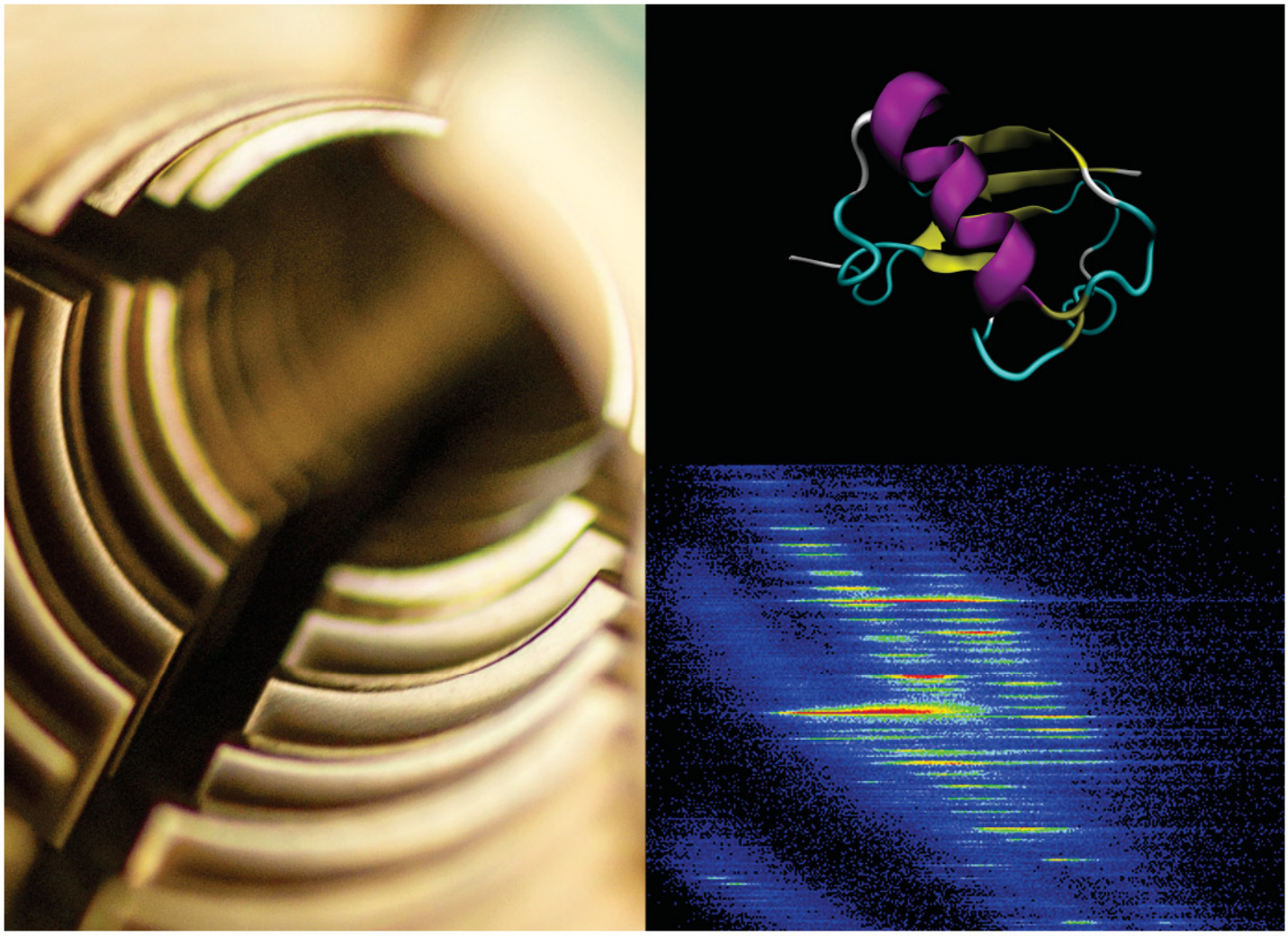

Showcasing collaborative research between the laboratories of Christian Bleiholder (Florida State University, USA) and Melvin A. Park (Bruker Daltonics Inc., USA).

Tandem trapped ion mobility spectrometry

Tandem trapped ion mobility spectrometry (TIMS-TIMS) was designed and analytically characterized. Its ability to select precursor ions, collisionally activate them to produce changes in conformation or fragmentation, and then mobility analyze the product ions offers novel approaches for bioanalytical applications.

As featured in:

See Christian Bleiholder *et al.*, *Analyst*, 2018, **143**, 2249.

ROYAL SOCIETY OF CHEMISTRY

rsc.li/analyst

Registered charity number: 207890

Analyst

PAPER

View Article Online
View Journal | View Issue

Cite this: *Analyst*, 2018, **143**, 2249

Tandem trapped ion mobility spectrometry†

Fanny C. Liu, ‡[a] Mark E. Ridgeway,‡[b] Melvin A. Park[b] and Christian Bleiholder *[a,c]

There is currently a strong interest in the use of ion mobility spectrometry-mass spectrometry (IMS-MS) instrumentation for structural biology. In these applications, momentum transfer cross sections derived from IMS-MS measurements are used to reconstruct the three-dimensional analyte structure. Recent reports indicate that additional structural information can be extracted from measuring changes in cross sections in response to changes of the analyte structure. To further this approach, we constructed a tandem trapped IMS analyser (TIMS-TIMS) and incorporated it in a QqTOF mass spectrometer. TIMS-TIMS is constructed by coupling two TIMS analysers *via* an "interface region" composed of two apertures. We show that peptide oligomers (bradykinin) and native-like protein (ubiquitin) ions can be preserved through the course of an experiment in a TIMS-TIMS analyser. We demonstrate the ability to collisionally-activate as well as to trap mobility-selected ions, followed by subsequent mobility-analysis. In addition to inducing conformational changes, we show that we can fragment low charge states of ubiquitin at >1 mbar between the TIMS analysers with significant sequence coverage. Many fragment ions exhibit multiple features in their TIMS spectra, which means that they may not generally exist as the most stable isomer. The ability of TIMS-TIMS to dissociate mobility-selected protein ions and to measure the cross sections of their fragment ions opens new possibilities for IMS-based structure elucidation.

Received 19th December 2017,
Accepted 20th March 2018

DOI: 10.1039/c7an02054f

rsc.li/analyst

Introduction

Ion mobility spectrometry-mass spectrometry (IMS-MS) is an established analytical technique that separates ions by differences in their ion mobility K and m/z ratio.[1,2] Many applications take advantage of the ability to determine the momentum transfer cross section of an analyte ion from its mobility according to[2,3]

$$\Omega = \frac{3q}{16N}\sqrt{\frac{2\pi}{\mu k_B T}}\frac{1}{K} \quad (1)$$

where K, q, and Ω are the mobility, charge, and cross section of the analyte ion, N and T the number density and temperature of the buffer gas, μ the reduced mass of the buffer gas and analyte ion, and k_B the Boltzmann constant.

Knowledge of ion cross sections has proven significant in many areas including identifying compound class and detailed structure.[4] Particularly relevant are structural biology applications where IMS-MS has demonstrated the ability to address many problems that are challenging to traditional biophysical methods.[5–8] For instance, IMS-MS cross section measurements were pivotal to elucidate structures for complex and dynamic biological systems such as amyloid assemblies,[9–11] viral capsids,[12] and other biological complexes.[13,14] Nevertheless, it remains highly challenging to infer a three-dimensional structure from a singular cross section measured by IMS-MS. This is rooted in the fact that a cross section is inherently an orientation-averaged (effective) area of the analyte[2,15–17] and thus does not directly contain detailed information about the three-dimensional structure of the analyte.

For this reason, it is often advantageous for structure elucidation to interpret *changes* in cross sections caused by *changes* in analyte structure as opposed to interpreting singular cross section values.[10,12,18,19] For example, cross sections of peptide assemblies increase linearly with oligomeric state for fibril-forming systems.[10,20] By contrast, peptide assemblies that grow isotropically exhibit a non-linear relationship between cross section and oligomeric state. What is important here is that growth-modes of peptide assemblies can be directly distinguished from observing the respective changes in cross sections.

One can also deliberately change the analyte structure by modulating the IMS operating settings and monitor how the ion cross section changes as a response. One approach is to measure cross section changes as the time scale of the IMS measurement is increased.[21–24] For example, Clemmer showed

[a]*Department of Chemistry and Biochemistry, Florida State University, Tallahassee, FL 32306-4390, USA. E-mail: cbleiholder@fsu.edu*
[b]*Bruker Daltonics Inc., 40 Manning Road, Billerica, MA, 01821, USA*
[c]*Institute of Molecular Biophysics, Florida State University, Tallahassee, FL 32306-4390, USA*

†Electronic supplementary information (ESI) available: Mass spectrum of ubiquitin sprayed with native condition, preparation of bradykinin and ubiquitin samples, detailed settings for mobility-selection, trapping, and activation experiments. See DOI: 10.1039/c7an02054f

‡These authors contributed equally.

that ubiquitin and cytochrome c ions with similar cross sections display divergent unfolding rate constants.[21,22] In a similar fashion, rates of structural transition of analyte ions can be determined by overtone mobility spectrometry (OMS).[25] Another strategy is to monitor changes in the cross section as ions are energetically activated by collisions with buffer gas particles.[19,26] Using this approach, Ruotolo recently showed that the number of unfolding transitions in the gas-phase is directly related to the number of protein domains in the solution.[26] In these cases, changes in cross section observed in response to changes in operating settings provide additional information about the three-dimensional analyte structure.

However, ion mobility spectra for biological systems can be complex. For instance, a specific charge state of small proteins[27–29] and even peptides[10,30–32] often contains multiple features. This complexity makes it difficult to unambiguously relate changes observed in ion mobility spectra to specific changes in molecular structure. This issue can be addressed by tandem IMS spectrometry (IMS-IMS) which allows the selection of ions with specific mobilities.[33] Bush has recently mobility-selected ions from cytochrome c and monitored structural changes of charge state +7 over time.[24] Previously, Clemmer demonstrated the ability to mobility-select and collisionally-activate a specific ion mobility peak and detect the resulting changes in cross section.[33,34] More recently, Rizzo and Clemmer have coupled this IMS-IMS capacity with cryogenic ion spectroscopy[35] and studied conformations of a bradykinin-derived peptide[36] and glycosaminoglycans subclasses.[37] These reports indicate that the ability to probe structural changes for mobility-selected ions can significantly facilitate the structural interpretation of ion mobility spectra. Nevertheless, tandem IMS instruments are currently used only by a few dedicated laboratories that are able to build and operate these systems.

Here, we report on the design and operation of a tandem trapped IMS instrument (TIMS-TIMS) incorporated in a QqTOF mass spectrometer. Owing to the TIMS method,[38–41] tandem TIMS commands a compact design, the ability for high resolving powers[42,43] and to preserve native-like protein structures.[29] Further, our instrument is capable to perform collisional-activation/dissociation and time-resolved IMS measurements for mobility-selected ions and has the additional capability for MS/MS analysis. We describe the design, operation, and characteristics of the TIMS-TIMS instrument and demonstrate the ability to preserve structure, select, trap, and collisionally activate analyte ions. In addition to inducing conformational changes, we fragment mobility-selected ubiquitin ions by collisional induced dissociation (CID), followed by mobility-analysis of the fragment ions. The results showcase the potential of TIMS-TIMS for biological applications.

Experimental design

Overview of TIMS-TIMS

A TIMS-TIMS device is incorporated in a prototype ESI-QqTOF mass spectrometer (Bruker Daltonics, Billerica, MA, USA). A schematic is shown in Fig. 1. The TIMS-TIMS device is constructed from two, dimensionally identical, TIMS analysers.[38–41] Each TIMS analyser, with an overall length of 154 mm, comprises three regions: an entrance funnel, an analyser tunnel, and an exit funnel.

Pumping

Four pumping ports are situated in the TIMS-TIMS device to control the pressure in the entrance and exit funnel regions of TIMS-1 (p1 and p2, respectively) and TIMS-2 (p3 and p4,

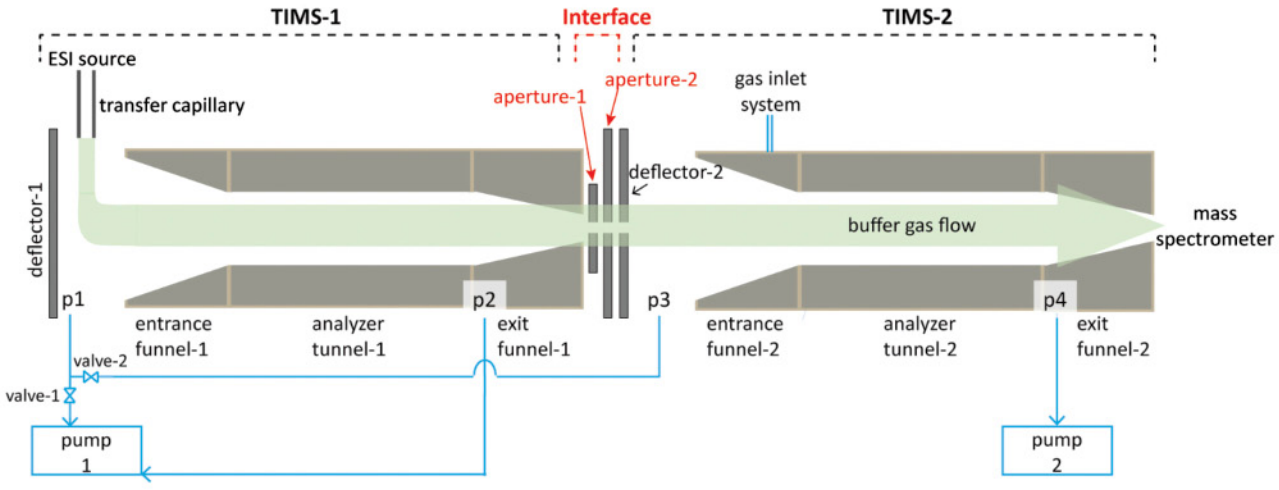

Fig. 1 Schematic of a TIMS-TIMS device. Two adjacent TIMS analysers are connected by an interface region comprising two apertures. Ions generated from electrospray enter the TIMS-TIMS device *via* the transfer capillary and are guided towards its exit by a gas stream and electric fields. TIMS-TIMS is capable to mobility-separate and mobility-select ions, as well as to activate and/or trap the selected ions followed by a subsequent mobility-analysis. DC and RF voltages applied to the TIMS analysers and the apertures in the interface are controlled independently from each other. Two rotary vane pumps and control valves establish the gas pressures at the entrance and exit regions of TIMS-1 (p1, p2) and TIMS-2 (p3, p4) to control the gas flow through TIMS-TIMS. A gas inlet system is optionally used to introduce a secondary buffer or reactant gas into TIMS-2.

respectively). Currently, the pressures p1 to p4 are set *via* two single stage 40 m^3 h^{-1} rotary vane pumps and manual control valves as indicated in Fig. 1. An inlet system exists directly in front of TIMS-2 (at p3) by which a secondary buffer gas can be introduced into TIMS-2. By adjusting the gas flow through the inlet system and setting p3 higher than p2, independent control of the composition of gas in TIMS-1 and TIMS-2 as well as the addition of a different buffer or reactant gas into TIMS-2 is possible by completely closing valve 2 (Fig. 1) and using p2 to remove the small amount of backflow from p3. Pressure p1 to p4 are monitored by means of Pirani gauges (Pfeiffer Vacuum, Germany). Pressures in the two entrance funnel regions (p1 and p3) typically range from 1–4 mbar.

Generation of ions and transfer into TIMS-TIMS

Ions are generated by electrospray ionization and enter TIMS-TIMS through a transfer capillary (Fig. 1). Ions are deflected by 90 degrees from the capillary exit into the ion funnel entrance by a deflector assembly of four 0.5 mm thick stainless steel dc-only deflector plates spaced 3.2 mm apart with an aperture of 25 mm leading into the entrance funnel of TIMS-1.

TIMS-1 and TIMS-2 analysers

The entrance funnels consist of 15 printed circuit boards (PCBs), starting with a diameter of 25.4 mm and linearly tapering to an 8 mm diameter over 48 mm. Each electrode is segmented into quadrants. A quadrupolar electric field is generated at each plate through the application of two radio frequency (rf) phases shifted by 180 degrees, with the phase between adjacent PCBs also shifted by 180 degrees in order to create a dipolar electric field along the length of the entrance funnel. All PCBs of each funnel are driven *via* a single rf generator running at 800–900 kHz and up to 350 Vpp. Each TIMS analyser is driven by separate rf generators to allow independent control of the rf amplitude. A direct-current (dc) electric field is created along the entrance funnel of each TIMS analyser by resistively dividing the potential difference between the first plate of the entrance funnel and the first plate of the analyser tunnel. The entrance funnel has 1.6 mm gaps between each element; however, the last 7 boards are sealed using 1.6 mm spacers and o-rings in an effort to smooth and better define gas flow as it enters the tunnel region.

The analyser tunnel consists of 26 PCBs with a diameter of 8 mm and a total length of 46 mm. A quadrupolar electric field is generated at each plate in the same fashion as in the entrance funnel; however, unlike the entrance and exit funnels, no phase shift occurs between PCBs. This creates a segmented linear quadrupole ion trap in which the TIMS analysis can take place. A dc electric field gradient is created over the first 13 plates to trap ions with a broad range in mobilities while the last 13 PCBs support the electric field plateau. The dc electric field within the tunnel scans during analysis by holding the exit of the tunnel at a fixed potential while the entrance potential changes with time.[38–41]

The exit funnel consists of 4 PCBs, starting with a diameter of 8 mm tapering to 4 mm over a total length of 11 mm. A quadrupolar field is generated at each plate in the same fashion as in the entrance funnel again with a 180 degree phase shift between PCBs. A dc electric field is created along the exit funnel by dividing the difference between the potential applied to the last element of the tunnel region and to aperture-1 (next element) using 180k ohm resistors between each plate. The dc electric field within the exit funnel is fixed during analysis. The exit funnel serves to both collect and focus ions exiting the TIMS analyser and provide a region to pump away the gas used for analysis *via* pumping ports p2 and p4.

Interface

Design. The two TIMS analysers in TIMS-TIMS are connected *via* an interface consisting of two apertures (Fig. 1). The apertures enable both mobility-selective ion gating and collisional-activation of mobility-selected ions. Aperture-1 is a 0.5 mm thick stainless steel plate with a 2 mm aperture located 1 mm from the last PCB of the exit funnel of TIMS-1. A second 0.5 mm thick stainless steel plate constitutes aperture-2, which has a 5 mm aperture and is positioned 2 mm after aperture-1, and 2 mm before the deflector of TIMS-2.

Ion gating. By timing the electric potentials at aperture-1 and aperture-2 with the mobility scan of TIMS-1, ions of a given mobility can either be transmitted by the application of (weakly) accelerating electric fields or blocked *via* repulsive electric fields. As the apertures are of small diameter and located 2 mm from one another, potential differences of only 10 V (50 V cm^{-1}) can be sufficient to completely block ions. Such low electric potentials, and the relatively low capacitance of the apertures themselves, allow switching times of less than 100 μs. This time scale is shorter than a single pulse of the time-of-flight mass analyser which serves as the clock for the TIMS measurements.

Ion activation. The interface consists of dc only elements, which are able to create a pure dc electric field. With the application of no or slightly accelerating electric fields, ions are transmitted through the interface region into the TIMS-2 analyser with no or little collisional activation. If desired, dc electric fields up to ~800 V cm^{-1} can be generated between aperture-1 and aperture-2, and up to ~600 V cm^{-1} between aperture-2 and deflector-2. The pressure in the interface region is on the order of 1–3 mbar.

Timing between TIMS-1, TIMS-2, aperture-1, aperture-2

Control of the TIMS-TIMS analyser is accomplished through custom software (Danielson Software Consulting, Richland, WA) which sets the dc voltages for each TIMS device while recording mass spectra and generating the 2D TIMS-MS data files. The dc voltages for TIMS are controlled through two USB-6289 digital to analog converters (National Instruments Corporation Austin, TX) and generated from an in-house built 8-channel dc supply capable of ±300 V and slew rates of 300 V ms^{-1}. The software allows the construction of TIMS scan functions, as well as to select mobility position (delay from the start of the ramp of TIMS-1) and mobility width (duration in

time) for which the gate will remain open. The resulting mass spectra for each step of the TIMS scan are acquired using a U1084 8-bit (Keysight Technologies, Santa Rosa, CA) digitizer recording at 1 GS s^{-1}.

Modes of operation

The TIMS-1 and TIMS-2 analysers can be operated independently from each other to: (1) transmit ions without mobility separation; (2) to separate ions based on their mobility; and (3) to trap ions for a specified time interval immediately prior to mobility-analysis. The interface between the TIMS analysers allows four modes of operation: (1) transmission; (2) mobility-selection; (3) collisional-activation/dissociation; and (4) mobility-selection combined with collisional-activation/dissociation of ions. These modes of operation in TIMS-1, the interface, and TIMS-2 can be combined to generate a number of different operational modes in the TIMS-TIMS device (Table 1). Additionally, the mass spectrometer system has the capability to perform MS/MS analysis.

Ion mobility separation. TIMS-TIMS can be operated with either or both TIMS analysers operating as mobility analysers. As described under Experimental Design, each TIMS analyser employed in TIMS-TIMS operates in the same fashion as a single TIMS device described elsewhere.[39–41] Briefly, a pressure difference between the entrance and exit regions of the TIMS analysers (p1/p2 and p3/p4 for TIMS-1 and TIMS-2, respectively, see Fig. 1) induces a stream of buffer gas through the analyser that pushes ions towards the exit funnel. The axial electric field gradient in the first half of the analyser tunnel creates a force that counteracts the force on the ions due to the collisions with the stream of buffer gas. As a result, ions are trapped axially at a location in the tunnel where they experience no net force. Ions with high mobility are trapped closer to the entrance and are spatially separated from ions with lower mobility, which are trapped further inside the tunnel. The electric field gradient is then gradually decreased to elute the ions into the second half of the tunnel. Ions with lower mobility are eluted, and reach the detector, earlier than ions with higher mobility.

With the interface in transmission-only mode, dc potentials are applied to aperture-1 and aperture-2 to guide ions into the entrance funnel of TIMS-2 without activation. When ions are mobility-separated in TIMS-1 and only transmitted through TIMS-2 (Mode 1A, Table 1), the dc potentials successively decrease in TIMS-2 (*i.e.* a low electric field gradient within the analyser of TIMS-2 that is insufficient to block or appreciable slow ions eluted from TIMS-1). Mobility-separation in TIMS-2 occurs as described for TIMS-1 above. More details on ion separation in TIMS are found elsewhere.[39–41]

Selection of ions with specified mobility. Selective transmission of ions within a specific mobility range can be performed in TIMS-TIMS (Modes 2A, 2B, and 3B, Table 1) by gating ions in the interface region. Ion gating is achieved by applying a transmitting dc voltage at aperture-2 for a specific period of time and a blocking dc voltage otherwise. The appropriate delay and duration time to select the mobility range of interest can be determined from a spectrum recorded in Mode 1A, where analyte ions are mobility-separated only in TIMS-1 and transmitted through the interface and TIMS-2. The minimum duration for ion gating is a single TOF pulse which is on the order of 144 μs for the measurements conducted here. Subsequent to mobility selection at the interface, ions can either be transmitted through TIMS-2 into the mass spectrometry region (Mode 2A) or undergo a second mobility separation in TIMS-2 (Mode 2B and 3B).

Collisional activation/dissociation of analyte ions. Ions can be collisionally activated and dissociated in the interface region of the TIMS-TIMS analyser by dc-only electric fields between aperture-1 and aperture-2 as well as between aperture-2 and deflector-2. Collisional activation can be performed either for the total mobility distribution (Mode 3A) or for mobility-selected ions (Mode 3B). Activated or fragmented ions can be either directly transmitted into the mass spectrometry region (Mode 3A) or undergo a second mobility separation in TIMS-2 to determine their mobilities (Mode 3B). If desired, ions can be additionally activated by dc/rf electric fields in the funnel regions of the TIMS analysers as described previously.[29]

Trapping of analyte ions in TIMS analysers. TIMS analyser radially confines ions by a quadrupolar rf electric field. This radial confinement enables trapping of ions immediately prior to mobility analysis as described previously.[44] In TIMS-TIMS, ion trapping can be conducted in either TIMS-1 and/or TIMS-2 as well as combined with any of the modes of operation described above.

MS/MS analysis. The TIMS-TIMS device is incorporated into a Bruker ESI-QqTOF Impact mass spectrometer which has the

Table 1 Typical operational modes of TIMS-1, interface, and TIMS-2[a]

	Interface	TIMS-2	Mode
Ion mobility separation (IMS)	Transmission	Transmission	1A[b]
	Transmission	Mobility-separation	1B[b]
			1C[c]
Selection of a narrow mobility range	Selection	Transmission	2A[b]
	Selection	Mobility-separation	2B[b]
Activation/dissociation of analyte ions	Activation/dissociation	Transmission	3A[b]
	Selection and activation/dissociation	Mobility-separation	3B[b]

[a] Both TIMS-1 and TIMS-2 analysers can also trap ions prior to mobility analysis. [b] Ion mobility separation occurs in TIMS-1. [c] Ions are transmitted through TIMS-1 without mobility separation.

capacity for MS/MS analysis after mobility separation by TIMS-TIMS. To this end, mobility-separated ions can be mass-selected in the quadrupole and collisionally activated in the collision cell. The MS/MS capability of the QqTOF mass spectrometer has been documented elsewhere[45] and is not illustrated here for brevity.

Results and discussion

Resolving power of TIMS-1 and TIMS-2 analysers

Theoretical considerations show that the resolving power of a TIMS analyser is given by[40,46]

$$R \approx v_g \sqrt[4]{\frac{2L_p}{\beta}} \frac{1}{\sqrt[4]{K^3}} \sqrt{\frac{q}{16 \ln 2 k_B T}} \quad (2)$$

where v_g is the gas velocity, L_p the length of the "plateau" region and β the rate of change of the electric field in the analyser, K and q are the mobility and charge of the analyte ion, T the gas temperature, and k_B the Boltzmann constant.

Fig. 2 characterizes the resolving powers observed for TIMS-1 and TIMS-2 in tandem TIMS. Fig. 2a shows a mass spectrum recorded for high concentration Agilent ESI tune mix. The arrival time distributions of m/z 622 (blue trace), 922 (pink trace), and 1522 (black trace) are converted into reduced mobility distributions as described[42] and each peak is fitted to a Gauss function (Fig. 2a, insets). The resulting K_0 and full-width at half maximum (FWHM) values are used to determine the resolving power. Fig. 2b correlates the resolving powers R observed in TIMS-1 and TIMS-2 for m/z 622 (blue triangles), m/z 922 (pink circles), and m/z 1522 (black squares) to $\beta^{-1/4}$, obtained with gas pressures of 3.4 and 1.2 mbar at p1 and p3. As expected from eqn (2), R increases linearly with $\beta^{-1/4}$. The resolving powers observed for TIMS-1 are slightly higher than the values reported by Michelmann *et al.* for a single TIMS analyser at a gas pressure of 3.1 mbar.[40] The resolving power of TIMS-2 is lower than in TIMS-1 in the experiments performed here, because the entrance pressure of TIMS-2 (p3 = 1.2 and 1.9 mbar) is lower than for TIMS-1 (p1 = 3.4 mbar). Nevertheless, the obtained resolving powers in TIMS-2 are comparable to a 2 m drift tube.[47] Moreover, if desired, the resolving power of either analyser can be further optimized by expanding the mobility scan time and/or employing a smaller electric field range in the analyser tunnel.[40]

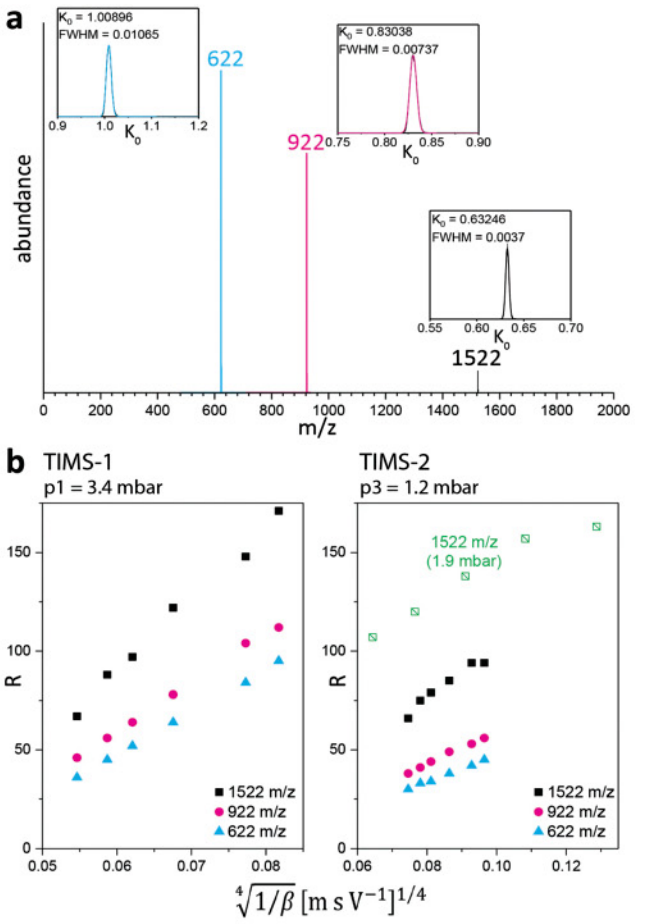

Fig. 2 Resolving power of the TIMS-1 and TIMS-2 analysers in tandem TIMS under typical operating conditions. (a) Mass spectrum of Agilent tune mix. Insets show ion mobility spectra for m/z 622 (blue trace), m/z 922 (pink trace), and m/z 1522 (black trace). (b) Resolving power of TIMS-1 and TIMS-2 for m/z 622 (blue triangles), 922 (pink circles), and 1522 (black squares) for different ramp rates β. The time scale of these measurements varies between 72 and 245 ms. The resolving power can be greatly increased by increasing entrance pressure and/or time-scale (green squares, p3 = 1.9 mbar, time scale up to 980 ms).

Preservation of native-like protein conformations

The ability of an ion mobility instrument to investigate biologically relevant questions relies on its ability to preserve native-like conformations present in the solution.[8] Previously, we demonstrated that a single TIMS device is able to retain native-like conformations of the protein ubiquitin.[29] However, we also observed that elevated dc and/or rf-electric fields can lead to denaturation of native-like structures. The TIMS-TIMS device described here contains a second TIMS analyser as well as an interface with supplementary dc and rf fields compared to a single TIMS device. Hence, we investigate the ability of TIMS-TIMS to preserve native-like ions of the protein ubiquitin.

The mass spectrum observed for ubiquitin under native electrospray conditions shows charge states +6, +7 and +8 (Fig. S1, ESI†); charge states <+6 and >+8 are not observed which is consistent with previous reports.[28] TIMS-TIMS settings to preserve native-like ions are optimized as described previously[29] (see ESI† for detailed experimental settings). First, we separate ions in TIMS-1 and transmit them through TIMS-2. The resulting ion mobility spectra are found in Fig. 3a. Charge state +6 is dominated by a single peak (1215 Å) while the spectra for +7 and +8 exhibit features in addition to a major peak (1272 and 1300 Å, respectively). Next, we transmit ions through TIMS-1 and mobility-separate them in TIMS-2. The corresponding ion mobility spectra (Fig. 3b) are highly similar to those when separation occurs only in TIMS-1

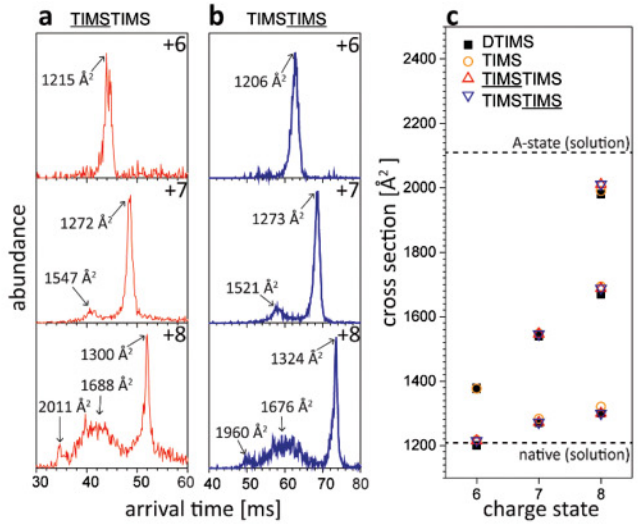

Fig. 3 Arrival time distributions and cross sections recorded for ubiquitin under native electrospray conditions with nitrogen as buffer gas. (a), (b) Arrival time distributions observed for ubiquitin ions under "soft" TIMS-TIMS settings. Note that in TIMS, ions with lower mobility exhibit shorter arrival times which is opposite to travelling wave and drift tube IMS systems. Ion separation occurs in TIMS-1 (a, red trace) as well as in TIMS-2 (b, blue trace). The spectra are dominated by a major peak corresponding to native-like structures. Minor features observed for the +7 and +8 ions correspond to (partially) unfolded features. (c) Cross sections of ubiquitin plotted as a function of charge state observed by TIMS-TIMS (red and blue triangles), TIMS (orange circle), and drift tube IMS (black square). Strong agreement between the three ion mobility systems is noted. The theoretical cross sections for the native and the A-state ubiquitin solution structures are indicated by dashed lines.

(Fig. 3a). The cross sections corresponding to the dominant peaks observed by TIMS-TIMS for ubiquitin +6, +7, and +8 are plotted in Fig. 3c as a function of the charge state and compared to cross sections previously reported for a single TIMS analyser[29] and the Bowers' drift tube.[48] We note a strong agreement between all data sets. Further, the cross sections for the main features in the +6, +7, and +8 spectra closely agree with the expected cross section of the native solution structure of ubiquitin (Fig. 3c, dashed line).[48] Overall, these observations illustrate that TIMS-TIMS is capable to preserve native-like protein conformations.

Mobility-selection of ions in the interface and trapping of mobility-selected ions in TIMS-2

We demonstrate the ability of TIMS-TIMS to select ions within a specific range of mobilities using bradykinin. To this end, singly-charged bradykinin ions are selected at aperture-2 in the interface as described in Experimental design.

We first perform mobility-separation in TIMS-1 and transmit ions through the interface and TIMS-2 (Mode 1A). The resulting mass spectrum is dominated by charge state +2 (m/z 531) and nominal charge state +1 (m/z 1061) of bradykinin (Fig. 4a). The ion mobility spectrum of the m/z 1061 peak displays multiple features which were previously[47,49] assigned as

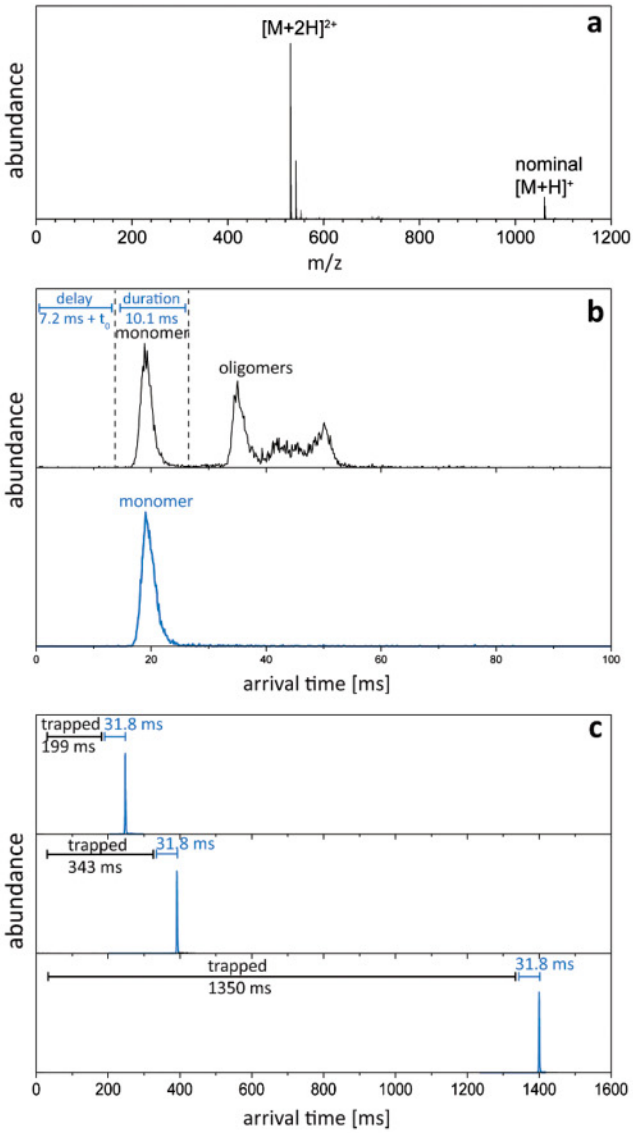

Fig. 4 Mobility selection and gas-phase trapping of singly charged bradykinin monomer in TIMS-TIMS. (a) Mass spectrum of bradykinin obtained with TIMS-TIMS/MS shows charge state +1 and +2. (b) (top) Arrival time distribution of bradykinin +1 obtained with Mode 1A shows several distinct peaks (black trace). (Bottom) To select the monomer peak of charge state +1 with Mode 2A, a transmitting dc voltage is applied at aperture-1 for a duration of 10.1 ms after a delay time of 7.2 ms (blue trace). See text for detailed information. (c) Arrival time distributions of the selected monomer peak when trapped over 199 ms (top), 343 ms (middle), and 1350 ms (bottom) in TIMS-2.

the singly-charged monomer and multiply-charged oligomers of bradykinin (Fig. 4b, top). Overall, the mass spectrum and the m/z 1061 ion mobility spectrum are consistent with previous reports using drift-tube IMS.[47,49] The ability of TIMS-TIMS to retain weakly-bound oligomers of bradykinin is an interesting observation in itself and deserves a detailed investigation in full length. Here, we focus on demonstrating the ability of TIMS-TIMS to mobility-select a single peak from an ion mobility spectrum that contains multiple features. We

determine the appropriate ion gating delay and duration to select only the singly-charged monomer species from the m/z 1061 ion mobility spectrum (Fig. 4b, top). Note that the arrival time distribution reflects the time ions arrive at the detector while the ion selection occurs in the interface. Thus, the time ions spend in TIMS-2 and the mass spectrometer region (t_0) has to be taken into account for the ion gating delay. Using Mode 2A, we apply a transmitting dc voltage at aperture-2 between 7.2 and 17.3 ms, which results in the selective transmission of the monomer peak (Fig. 4b, bottom).

TIMS-TIMS is also capable of trapping a mobility-selected ion population in the TIMS-2 analyser prior to mobility-analysis. To this end, we select the singly-charged bradykinin monomer as described above and trap these ions in TIMS-2 for a specified duration prior to mobility-analysis. Fig. 4c shows the recorded ion mobility spectra resulting from trapping the selected singly-charged bradykinin monomers for 199, 343, and 1350 ms in TIMS-2 immediately prior to mobility-analysis. The recorded ion mobility spectra for all three trap times are dominated by a single peak which appears at the same scan time in TIMS-2 (31.8 ms, see Fig. 4c). Overall, Fig. 4c illustrates the capability of TIMS-TIMS to mobility-select ions from a parent distribution and to trap the selected ions in TIMS-2 for a defined period of time before mobility-analysis.

Collisional activation of mobility-selected protein ions

We use charge state +7 of ubiquitin to illustrate the ability of TIMS-TIMS to mobility-select and then collisionally-activate a specific protein conformation. Note that we electrospray from a non-native solution in order to produce multiple ubiquitin conformations and to emphasize the ability to mobility-select and activate a single feature from a complex arrival time distribution.

Ubiquitin ions are mobility-selected as described above for bradykinin. First, we record the arrival time distribution in TIMS-1 and transmit ions through the interface region and TIMS-2 (Fig. 5a, black trace). The recorded arrival time distribution for ubiquitin +7 exhibits two broad features from ~30–50 ms and ~50–60 ms. The feature observed at shorter arrival times corresponds to more extended structures with cross sections centered at ~1570 Å^2 while the feature observed between ~50–60 ms corresponds to more compact structures with a cross section of ~1300 Å^2. We select the compact feature by transmitting ions through the interface between 47.5 and 59.7 ms and setting a blocking potential at aperture-2 otherwise (Fig. 5a, blue trace). Mobility-analysis in TIMS-2 reveals a single feature at ~93–96 ms which corresponds to cross sections of ~1300 Å^2 as expected (Fig. 5b).

To collisionally activate the selected ions, we increase the electric field strength between aperture-2 and deflector-2. Subsequently, we perform mobility-analysis in TIMS-2 to detect structural changes of ubiquitin ions resulting from collisional-activation. Fig. 5c–f display ion mobility spectra obtained with a dc bias of 20 to 50 V between aperture-2 and deflector-2. Ions with cross sections of ~1300 Å^2 dominate the spectra for a dc activation voltage up to 30 V (Fig. 5c and d),

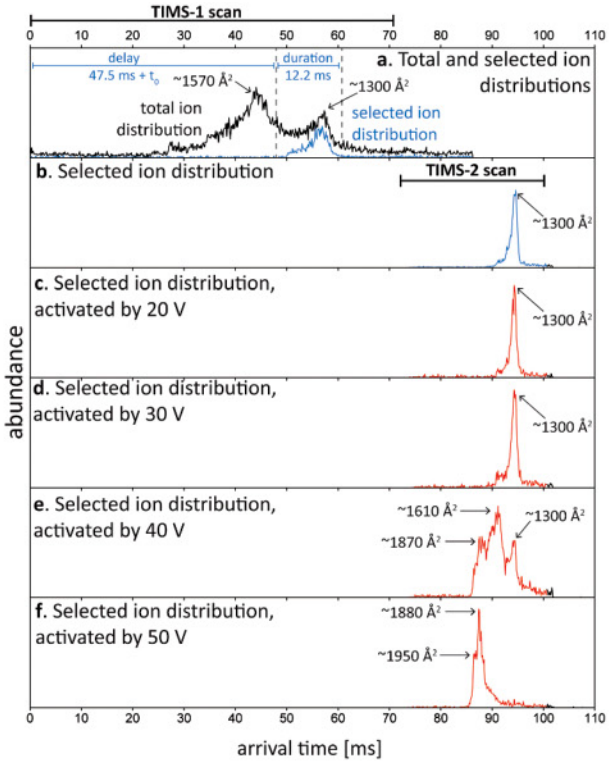

Fig. 5 Mobility selection and collisional activation of compact ubiquitin +7 ions in TIMS-TIMS. (a) Arrival time distribution of ubiquitin +7 ions from a non-native solution is obtained with Mode 1A (black trace). To mobility-select the compact peak, ions are gated with a delay and duration time of 47.5/12.2 ms (Mode 2A, blue trace). (b) Arrival time distribution of selected compact peak, obtained with Mode 2B. (c–f) Selected compact ions were then activated by a DC potential of (c) 20 V, (d) 30 V, (e) 40 V, and (f) 50 V between aperture-2 and deflector-2. Extended conformations dominate the ion distribution for dc potential >30 V.

which agrees well with the initial mobility-selected ion population (Fig. 5a and b). For larger dc biases, we observe that the ion abundances shift significantly towards shorter arrival times. Fig. 5e shows that two new features appear at 40 V dc bias with arrival times between ~85–88 ms (~1870 Å^2) and 88–93 ms (~1610 Å^2) but the original ion population with a cross section of ~1300 Å^2 is still present in the spectrum. At a dc bias of 50 V (Fig. 5f), a significant abundance of the original ion population is no longer observed. Instead, the spectrum is dominated by strongly extended conformations with cross sections of ~1880 Å^2 and ~1950 Å^2, respectively. These extended cross sections correspond well with literature values for elongated conformations of ubiquitin observed by TIMS[43] and drift tube IMS.[50] Hence, the data show that compact ubiquitin +7 ions change their conformation when activated by a dc bias of >30 V between aperture-2 and deflector-2. In sum, Fig. 5 demonstrates the ability of TIMS-TIMS to collisionally activate a mobility-selected population of ubiquitin ions with a well-defined dc activation energy in the interface, and to detect the resulting changes in the analyte cross sections.

Collisional induced dissociation of mobility-selected protein ions

We demonstrate the ability of tandem TIMS to dissociate intact proteins into fragment ions in the interface by collision-induced dissociation (CID). To this end, we transmit ions from electrosprayed ubiquitin with ion gating delay and duration of 25.9 and 4.3 ms at aperture-2 in the interface, which correspond to the extended ubiquitin +8 conformer (Fig. 6a–c). Minor abundances of +5 to +7 ions were also transmitted to TIMS-2. We subsequently increase the voltage between aperture-2 and deflector-2 up to 260 V. The obtained mass spectra show a sharp drop in abundance of +8 ions between 170 and 190 V and nearly a depletion of +6 to +8 ions between 200 V to 260 V (Fig. 6d and Fig. S2 in the ESI†). The decrease in abundance of $[M + nH]^{n+}$ ions correlates with emergence of fragment ions (Fig. 6d) while charge-stripping processes appear insignificant (Fig. S2†). We note high sequence coverage at activation voltages above 200 V, with mostly b and y-type ions including their H_2O and NH_3-loss ions (Fig. 6d and S3†). Extensive formation of y_{58}^{+5} and y_{40}^{+4} ions, resulting from cleavage N-terminal to Pro19 and Pro37, are observed with activation voltage >180 V. We obtain similar results when selecting and fragmenting compact +7 ions (data not shown for brevity).

To our best knowledge, this is the first report on CID of a low charge state of an intact protein above ~1 mbar with significant sequence coverage. CID between two IMS drift tubes above ~1 mbar in helium was reported for peptides and other low molecular weight ions.[51–53] But fragmentation of ubiquitin was reported only for charge state +13 under these conditions and here cleavage at Pro19 predominated.[51] By contrast, we observe an array of fragment ions resulted from dissociation of ubiquitin +6 to +8 in tandem TIMS (Fig. 6c and d). We attribute this to the use of nitrogen as a buffer gas, which results in significantly higher collision energies than in collisions with helium atoms.[29]

Fig. 6e shows spectra recorded in TIMS-2 for the y_{40}^{+4} and y_{58}^{+5} fragment ions for different activation voltages. We observe two peaks in the spectra, which can be rationalized in several ways. First, the presence of two peaks could mean that the fragment ions exist as one structural isomer but that annealing into the most stable gas phase conformation is slower than the TIMS experiment. For example, the peaks could be due to *cis*/*trans* isomers of peptide bonds that have recently been proposed for peptide[36,54] and protein ions.[55] It is also conceivable that the different peaks result from different protonation sites or the presence of salt bridges. Furthermore, the two peaks could mean that the fragment ions exist as different structural isomers, similar to linear and cyclic isomers that were reported for a and b-ions of peptides.[56–58]

The ability of TIMS-TIMS to mobility-select and dissociate low charge states of proteins and to measure the mobilities of their fragment ions is potentially significant also from an analytical perspective. First, the fragmentation of full length protein ions in the interface of TIMS-TIMS could enable middle-down, or even top-down, proteomics experiments in which specific proteoforms are mobility-selected and fragmented, followed by mobility-analysis of their fragment ions. Second, it is tempting to contemplate if cross sections of protein (complex) fragment ions could be used as additional constraints to elucidate the precursor ion structure. Whether

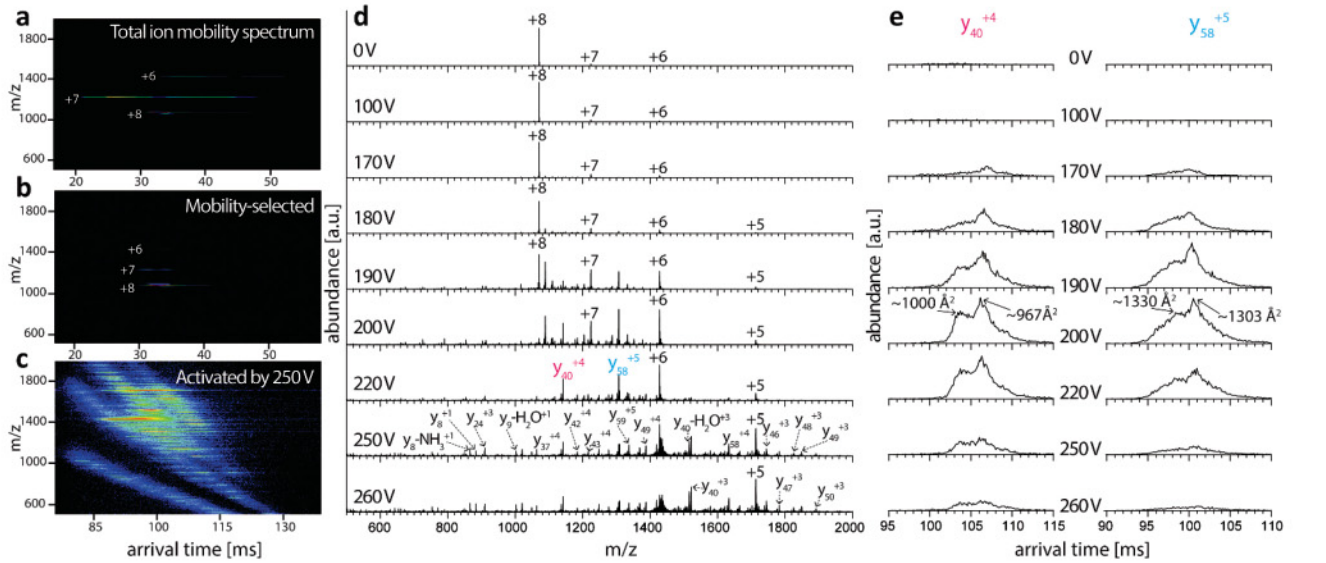

Fig. 6 Collision-induced dissociation of ubiquitin in the interface of tandem TIMS. (a–c) Nested IMS-MS spectra of electrosprayed ubiquitin without mobility-selection (a), with mobility-selection in the interface (b), with mobility-selection followed by collisional activation in the interface at 250 V (c). Mobility analysis conducted at TIMS-1 (a), (b) and at TIMS-2 for (c). (d) Mass spectra obtained from mobility-selection followed by collisional-activation of ubiquitin ions in the interface with activation voltages of 100–260 V. Dissociation of precursor ions are observed for activation voltage >170 V, with abundant formation of fragment ions and near depletion of the $[M + nH]^{n+}$ precursor ions as we increase the activation voltage to 260 V. (e) Ion mobility spectra recorded in TIMS-2 for the y_{40}^{+4} and y_{58}^{+5} fragment ions as a function of activation voltage. The spectra reveal two distinct conformations for both fragment ions.

or not this will turn out analytically useful depends on what these fragment ion structures are and how they are related to the precursor ion structure. The observation that protein fragment ions exist as more than one isomer suggests that CID in the TIMS-TIMS interface is not an idealized "slow heating" process and one might speculate that some aspects of the precursor ion structures might be retained during the fragmentation process. We will explore these questions in future publications.

Conclusion

Tandem TIMS (TIMS-TIMS) coupled with mass spectrometry is a potentially useful tool for the field of structural biology. Here incorporated in a QqTOF mass spectrometer, TIMS-TIMS consists of two trapped ion mobility spectrometry analysers connected *via* an interface comprising two aperture plates. Using bradykinin and ubiquitin as test cases, we demonstrated that peptide oligomers (bradykinin) and native-like protein (ubiquitin) ions can be preserved through the course of a TIMS-TIMS analysis. Further, we demonstrated the ability of TIMS-TIMS to select, trap, and collisionally activate ions. In particular, we selected and collisionally activated ubiquitin ions in the interface of tandem TIMS. Low activation potentials (30–50 V) result in the unfolding of compact ions into elongated structures, while high activation potentials (170–260 V) are sufficient to dissociate low charge states of ubiquitin at significant sequence coverage. Many fragment ions are found to exist in different structures.

In sum, the instrument described here couples the ability for tandem IMS analysis with collisional activation and dissociation as well as time-resolved measurements at high IMS resolving power. These capabilities of TIMS-TIMS open up new possibilities to elucidate structures of macromolecules by correlating changes in cross sections to energetics and kinetics of collision-induced unfolding and dissociation processes.

Conflicts of interest

There are no conflicts to declare.

Acknowledgements

This work was supported by the National Science Foundation under grant CHE-1654608.

Notes and references

1 H. H. Hill Jr., W. F. Siems and R. H. St. Louis, *Anal. Chem.*, 1990, **62**, 1201A–1209A.
2 E. A. Mason and E. W. McDaniel, *Transport Properties of Ions in Gases*, Wiley, New York, 1988.
3 H. E. Revercomb and E. A. Mason, *Anal. Chem.*, 1975, **47**, 970–983.
4 J. C. May, C. R. Goodwin, N. M. Lareau, K. L. Leaptrot, C. B. Morris, R. T. Kurulugama, A. Mordehai, C. Klein, W. Barry, E. Darland, G. Overney, K. Imatani, G. C. Stafford, J. C. Fjeldsted and J. A. McLean, *Anal. Chem.*, 2014, **86**, 2107–2116.
5 J. L. Benesch and B. T. Ruotolo, *Curr. Opin. Struct. Biol.*, 2011, **21**, 641–649.
6 G. R. Hilton and J. L. P. Benesch, *J. R. Soc., Interface*, 2012, **9**, 801–816.
7 T. Wyttenbach, N. A. Pierson, D. E. Clemmer and M. T. Bowers, *Annu. Rev. Phys. Chem.*, 2014, **65**, 175–196.
8 C. Bleiholder and M. T. Bowers, *Annu. Rev. Anal. Chem.*, 2017, **10**, 365–386.
9 S. L. Bernstein, N. F. Dupuis, N. D. Lazo, T. Wyttenbach, M. M. Condron, G. Bitan, D. B. Teplow, J.-E. Shea, B. T. Ruotolo, C. V. Robinson and M. T. Bowers, *Nat. Chem.*, 2009, **1**, 326–331.
10 C. Bleiholder, N. F. Dupuis, T. Wyttenbach and M. T. Bowers, *Nat. Chem.*, 2011, **3**, 172–177.
11 C. Bleiholder, T. D. Do, C. Wu, N. J. Economou, S. S. Bernstein, S. K. Buratto, J.-E. Shea and M. T. Bowers, *J. Am. Chem. Soc.*, 2013, **135**, 16926–16937.
12 C. Uetrecht, I. M. Barbu, G. K. Shoemaker, E. van Duijn and A. J. R. Heck, *Nat. Chem.*, 2011, **3**, 126–132.
13 B. T. Ruotolo, K. Giles, I. Campuzano, A. M. Sandercock, R. H. Bateman and C. V. Robinson, *Science*, 2005, **310**, 1658–1661.
14 M. Zhou, A. Politis, R. B. Davies, I. Liko, K.-J. Wu, A. G. Stewart, D. Stock and C. V. Robinson, *Nat. Chem.*, 2014, **6**, 208–215.
15 A. A. Shvartsburg and M. F. Jarrold, *Chem. Phys. Lett.*, 1996, **261**, 86–91.
16 T. Wyttenbach, G. von Helden, J. J. Batka, D. Carlat and M. T. Bowers, *J. Am. Soc. Mass Spectrom.*, 1997, **8**, 275–282.
17 C. Bleiholder, T. Wyttenbach and M. T. Bowers, *Int. J. Mass Spectrom.*, 2011, **308**, 1–10.
18 G. von Helden, N. G. Gotts and M. T. Bowers, *Nature*, 1993, **363**, 60–63.
19 D. E. Clemmer and M. F. Jarrold, *J. Mass Spectrom.*, 1997, **32**, 577–592.
20 T. D. Do, N. E. C. de Almeida, N. E. LaPointe, A. Chamas, S. C. Feinstein and M. T. Bowers, *Anal. Chem.*, 2016, **88**, 868–876.
21 E. R. Badman, C. S. Hoaglund-Hyzer and D. E. Clemmer, *Anal. Chem.*, 2001, **73**, 6000–6007.
22 S. Myung, E. R. Badman, Y. J. Lee and D. E. Clemmer, *J. Phys. Chem. A*, 2002, **106**, 9976–9982.
23 S. R. Harvey, J. Yan, J. M. Brown, E. Hoyes and V. H. Wysocki, *Anal. Chem.*, 2016, **88**, 1218–1221.
24 S. J. Allen, R. M. Eaton and M. F. Bush, *Anal. Chem.*, 2017, **89**, 7527–7534.
25 S. Lee, M. A. Ewing, F. M. Nachtigall, R. T. Kurulugama, S. J. Valentine and D. E. Clemmer, *J. Phys. Chem. B*, 2010, **114**, 12406–12415.
26 Y. Zhong, L. Han and B. T. Ruotolo, *Angew. Chem., Int. Ed.*, 2014, **53**, 9209–9212.

27 K. B. Shelimov and M. F. Jarrold, *J. Am. Chem. Soc.*, 1997, **119**, 2987–2994.
28 T. Wyttenbach and M. T. Bowers, *J. Phys. Chem. B*, 2011, **115**, 12266–12275.
29 F. C. Liu, S. R. Kirk and C. Bleiholder, *Analyst*, 2016, **141**, 3722–3730.
30 T. Wyttenbach, G. von Helden and M. T. Bowers, *J. Am. Chem. Soc.*, 1996, **118**, 8355–8364.
31 S. J. Valentine, A. E. Counterman, C. S. Hoaglund-Hyzer and D. E. Clemmer, *J. Phys. Chem. B*, 1999, **103**, 1203–1207.
32 R. R. Hudgins and M. F. Jarrold, *J. Am. Chem. Soc.*, 1999, **121**, 3494–3501.
33 S. L. Koeniger, S. I. Merenbloom, S. J. Valentine, M. F. Jarrold, H. R. Udseth, R. D. Smith and D. E. Clemmer, *Anal. Chem.*, 2006, **78**, 4161–4174.
34 N. A. Pierson, S. J. Valentine and D. E. Clemmer, *J. Phys. Chem. B*, 2010, **114**, 7777.
35 A. Masson, M. Z. Kamrath, M. A. S. Perez, M. S. Glover, U. Rothlisberger, D. E. Clemmer and T. R. Rizzo, *J. Am. Soc. Mass Spectrom.*, 2015, **26**, 1444–1454.
36 L. Voronina, A. Masson, M. Kamrath, F. Schubert, D. Clemmer, C. Baldauf and T. Rizzo, *J. Am. Chem. Soc.*, 2016, **138**, 9224–9233.
37 N. Khanal, C. Masellis, M. Z. Kamrath, D. E. Clemmer and T. R. Rizzo, *Anal. Chem.*, 2017, **89**, 7601–7606.
38 F. A. Fernandez-Lima, D. A. Kaplan and M. A. Park, *Rev. Sci. Instrum.*, 2011, **82**, 126106.
39 D. R. Hernandez, J. D. DeBord, M. E. Ridgeway, D. A. Kaplan, M. A. Park and F. Fernandez-Lima, *Analyst*, 2014, **139**, 1913.
40 K. Michelmann, J. A. Silveira, M. E. Ridgeway and M. A. Park, *J. Am. Soc. Mass Spectrom.*, 2015, **26**, 14–24.
41 C. Bleiholder, *Int. J. Mass Spectrom.*, 2016, 399–400.
42 J. A. Silveira, M. E. Ridgeway and M. A. Park, *Anal. Chem.*, 2014, **86**, 5624–5627.
43 M. E. Ridgeway, J. A. Silveira, J. E. Meier and M. A. Park, *Analyst*, 2015, **140**, 6964–6972.
44 E. R. Schenk, M. E. Ridgeway, M. A. Park, F. Leng and F. Fernandez-Lima, *Anal. Chem.*, 2014, **86**, 1210–1214.
45 H. R. Morris, T. Paxton, A. Dell, J. Langhorne, M. Berg, R. S. Bordoli, J. Hoyes and R. H. H. Bateman, *Rapid Commun. Mass Spectrom.*, 1996, **10**, 889–896.
46 J. A. Silveira, K. Michelmann, M. E. Ridgeway and M. A. Park, *J. Am. Soc. Mass Spectrom.*, 2016, **27**, 585–595.
47 P. R. Kemper, N. F. Dupuis and M. T. Bowers, *Int. J. Mass Spectrom.*, 2009, **287**, 46–57.
48 C. Bleiholder, N. R. Johnson, S. Contreras, T. Wyttenbach and M. T. Bowers, *Anal. Chem.*, 2015, **87**, 7196–7203.
49 A. E. Counterman, S. J. Valentine, C. A. Srebalus, S. C. Henderson, C. S. Hoaglund and D. E. Clemmer, *J. Am. Soc. Mass Spectrom.*, 1998, **9**, 743–759.
50 M. F. Bush, Z. Hall, K. Giles, J. Hoyes, C. V. Robinson and B. T. Ruotolo, *Anal. Chem.*, 2010, **82**, 9557–9565.
51 S. I. Merenbloom, S. L. Koeniger, S. J. Valentine, M. D. Plasencia and D. E. Clemmer, *Anal. Chem.*, 2006, **78**, 2802–2809.
52 S. I. Merenbloom, B. C. Bohrer, S. L. Koeniger and D. E. Clemmer, *Anal. Chem.*, 2007, **79**, 515–522.
53 B. C. Bohrer and D. E. Clemmer, *Anal. Chem.*, 2011, **83**, 5377–5385.
54 N. A. Pierson, L. Chen, D. H. Russell and D. E. Clemmer, *J. Am. Chem. Soc.*, 2013, **135**, 3186–3192.
55 S. Warnke, C. Baldauf, M. T. Bowers, K. Pagel and G. von Helden, *J. Am. Chem. Soc.*, 2014, **136**, 10308–10314.
56 A. G. Harrison, A. B. Young, C. Bleiholder, S. Suhai and B. Paizs, *J. Am. Chem. Soc.*, 2006, **128**, 10364–10365.
57 C. Bleiholder, S. Osburn, T. D. Williams, S. Suhai, M. Van Stipdonk, A. G. Harrison and B. Paizs, *J. Am. Chem. Soc.*, 2008, **130**, 17774–17789.
58 N. C. Polfer, B. C. Bohrer, M. D. Plasencia, B. Paizs and D. E. Clemmer, *J. Phys. Chem. A*, 2008, **112**, 1286–1293.